

# Modelling the influence of machined surface roughness on the fatigue life of aluminium alloy

**M. Suraratchai, J. Limido, C. Mabru\*, R. Chieragatti**

*Ecole Nationale Supérieure d'Ingénieurs de Constructions Aéronautiques*

*1, Place Emile Blouin, 31056 Toulouse, France*

\* Corresponding author: [catherine.mabru@ensica.fr](mailto:catherine.mabru@ensica.fr)

## Abstract

The influence of machined surface roughness on the fatigue life of 7010 aluminium alloy has been investigated. Four-point bending specimen have been machined according to various machining conditions and tested in fatigue. In order to explain the high dependence of SN curves on the surface roughness of the specimen, an approach based on the finite element analysis of measured surface topography is proposed. Surface grooves due to machining are supposed to generate stress concentrations that are so calculated. A model of fatigue life prediction is developed, using this definition of local  $K_t$ .

**Keywords:** Surface roughness; Machining; Aluminium alloy; Finite element method; Fatigue life.

## 1. Introduction

Fatigue life of structures is known to highly depend on the surface quality. Consequently, a great attention is paid to the specification and the realization of surfaces of machined parts when those must be dimensioned in fatigue. Three parameters are usually proposed to describe surface condition: i) a geometrical parameter: surface roughness; ii) a mechanical parameter: residual stress; iii) a metallurgical parameter: microstructure. These parameters

can vary separately according to the machining conditions. In engineering design, the effects of these parameters are commonly accounted for by using empirical reduction factors which modify the endurance limit of the material [1-2]. Reduction factors are defined for each type of machining process. Moreover, within each category of machining process the use of these reduction factors leads to surface specifications (generally in terms of roughness) linked to machining parameters such as tool shape, feed rate... Even if giving satisfactory fatigue life predictions, the use of this empirical method has obviously limitations due to its restricted area of validity. Indeed, changing machining process or machining parameters must then be accompanied by a new definition of reduction factors and/or surface specifications that must be validated by performing new fatigue tests. This constitutes a real problem as machining processes are in constant evolution in order to increase productivity.

In this context, the present study deals with the influence of machined surface quality on the fatigue strength of an aluminium alloy and aims to provide a mean to easily predict fatigue life when changing machining parameters without relying on empirical relations established by time-consuming and expensive fatigue tests. In the case of this alloy, surface roughness appears to be the predominant parameter affecting fatigue life and the present work focuses on the modelling of the effect of this parameter.

Surface roughness is usually characterized through average geometric parameters such as  $R_a$  (average roughness),  $R_y$  (peak-to-valley height roughness) or  $R_z$  (10-point roughness). These parameters are defined in terms of the profile height distribution ( $z$ ) recorded, in respect to the mean line, over an assessment length ( $L$ ) according to

$$R_a = \frac{1}{l} \int_0^l |z(x)| dx \quad (1)$$

$$R_y = |z_{\max} - z_{\min}| \quad (2)$$

$$R_z = \frac{1}{5} \left[ \sum_{i=1}^5 (z_i)_{\max} + \sum_{j=1}^5 |(z_j)_{\min}| \right] \quad (3)$$

where  $(z_i)_{\max}$  and  $(z_j)_{\min}$  are the 5 higher local maxima and lower local minima, respectively, of the profile height distribution  $(z)$ .

This kind of standard roughness parameters constitutes a simple and useful way of quantifying profile height distributions but it is not able to provide all specific features of the surface height distribution that are important to fatigue life. Beyond the early studies [3-5] leading essentially to empirical conclusions, several approaches to model the effects of geometric surface conditions on the fatigue strength of structures have been proposed. Most of them consider surface roughness in terms of stress concentration effect similar to a notch effect. This stress concentration effect can be described through the fatigue stress concentration factor  $K_f$  defined as the ratio between the fatigue limit of an un-notched (smooth) specimen and the fatigue limit of a notched (rough) specimen.

$$K_f = \frac{\sigma_D(\text{smooth})}{\sigma_D(\text{rough})} \quad (4)$$

$K_f$  can be related to the stress concentration factor  $K_t$  according to [6]

$$K_f = 1 + q(K_t - 1) \quad (5)$$

where  $q$  is the notch sensitivity, depending on the material and asperities geometry.

In this framework, Arola and Williams [7] proposed to estimate the stress concentration factor according to

$$K_t = 1 + n \left( \frac{R_a}{\rho} \right) \left( \frac{R_y}{R_z} \right) \quad (6)$$

where  $\rho$  is the effective profile valley radius of the surface texture and  $n$  represents the stress state ( $n=1$  for shear and  $n=2$  for tension). In the case of AISI 4130 CR steel [8], this expression provides better estimation of the fatigue stress concentration factor ( $K_f$ ) than the expression proposed by Neuber where

$$K_t = 1 + n \sqrt{\lambda \frac{R_z}{\rho}} \quad (7)$$

where  $\lambda$  refers to the ratio between spacing and depth of the asperities and is quite difficult to establish for machined surface textures. As et al. [9] proposed to calculate  $K_t$  from FE (Finite Element) simulations of the measured surface topography. They show that, in the case of an aluminium alloy, the use of  $K_f$ , originally developed for the fatigue limit, yields satisfactory prediction in a narrow life time region but cannot be applied for the whole life region.

Murakami [10] considered surface roughness as surface defect and defined a parameter related to the area of the periodic defects. Fatigue limit is then calculated through an empirical relation using this parameter and material hardness ( $H_v$ ). Another approach is based on non-propagation threshold [11] using fracture mechanics applied to short cracks. Comparing this approach to the  $K_f$  approach, Taylor and Clancy [12] concluded that for high roughness surfaces, notch effect approach is better while for low roughness surfaces fracture mechanics approach leads to better results. Andrews and Sehitoglu [13] proposed a computer model for fatigue crack growth from rough surfaces based on the Paris law using the effective stress intensity factor  $\Delta K_{eff}$  accounting for crack closure effect. Influence of roughness is directly taken into account through stress concentration factor  $K_t$  for short cracks while it is included in the effective crack length used for crack propagation law of long cracks. The authors calculated  $K_t$  by modifying Peterson Handbook [6] expression to apply to multiple elliptical notches that are not at equal distances. Comparing their results to experimental results for rough milled and ground 4340 steel specimens, they concluded to good correlation despite the large experimental scatter in lives. However, in the case of polished or fine milled specimens, due to fracture mechanisms from inclusions, the model should not be applicable.

In the present paper, surface roughness is considered as generating local stress concentration governing surface crack propagation or non-propagation. This approach requires the

calculation of the stress concentration factor  $K_t$ . Similarly to the method proposed by As et al. [9]  $K_t$  is estimated by the finite element analysis of measured surface topographies. For fatigue limit, this so-calculated stress concentration factor is integrated in a non-propagation threshold approach. For limited fatigue lives, propagation life time ( $N_p$ ) and initiation life time ( $N_i$ ) are distinguished:  $K_t$  is used in a Basquin [14] type power law for evaluating  $N_i$ ; an estimation of  $N_p$  is obtained integrating  $K_t$  in a Paris law and considering the stress concentration only affects surface crack propagation. This model is established based on academic surfaces generated by a shaper and is validated on industrial specimens with surfaces obtained by numerous and various machining processes leading to different surface roughnesses.

## 2. Experimental

### 2.1. Material

The material investigated in this paper is a 7010-T7451 aluminium alloy whose composition is presented in Table 1.

	Si	Fe	Cu	Mn	Mg	Cr	Zn	Ni	Zr	Ti	Al
Min	-	-	1.5	-	2.1	-	5.7	-	0.10	-	Balance
Max	0.12	0.15	2	0.10	2.6	0.05	6.7	0.05	0.16	0.06	Balance

**Table 1 : Chemical composition of 7010 aluminium alloy (wt %)**

It was provided in the form of a rolled plate of 70mm thickness. The microstructure is composed of grains that are highly elongated in the rolling direction. Three directions can be defined as presented in Figure 1. Grain size is about 350 $\mu$ m in the rolling direction, L, and about 150 $\mu$ m and 60 $\mu$ m in T and S direction respectively.  $Al_7Cu_2Fe$  and  $Mg_2Si$  intermetallic particles of 8-10 $\mu$ m size can be found regularly in the microstructure and are located in

recrystallized grains. These grains are smaller than the previous grains: 80, 60 and 40  $\mu\text{m}$  in L, T and S directions respectively.

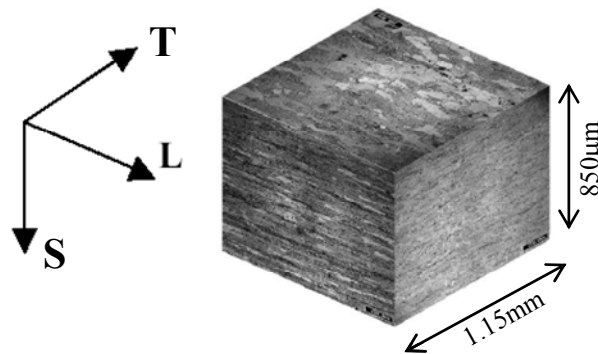
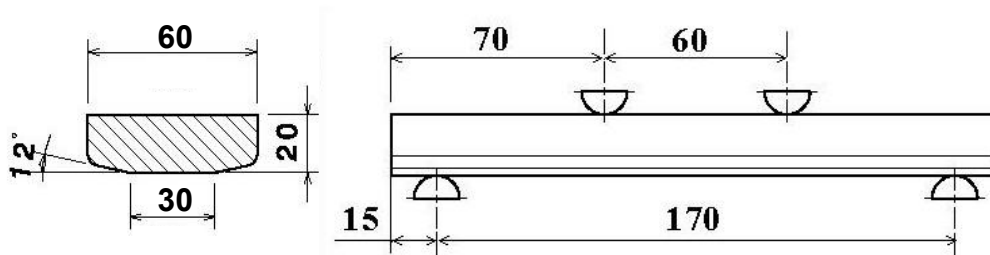


**Figure 1 : Microstructure of rolled 7010-T74511 aluminium alloy**

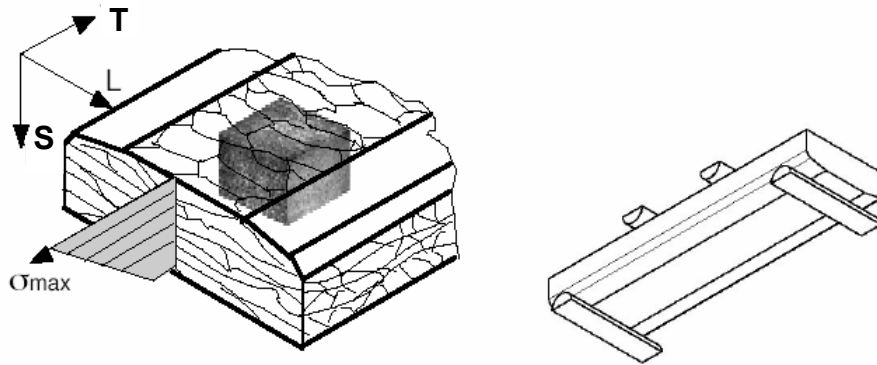
## 2.2. Specimens and surface preparation

Four-point bending fatigue tests were carried out on specimens shown in Figure 2. Shape and dimensions of these specimens correspond to the industrial partner standards. Chamfers on the side in tension are introduced to avoid fatigue crack starting from specimen corners.

Specimens are taken in the plate so that the stress induced by four-point bending is parallel to the T direction as seen in Figure 3.

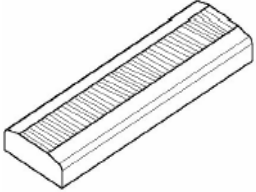
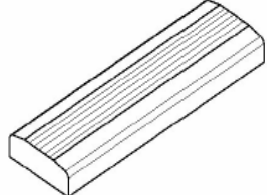


**Figure 2 : Fatigue specimens geometry**



**Figure 3 : Microstructure orientation of the specimen with respect to loading condition**

Two types of specimens were considered: on one hand, specimens provided by an industrial partner and made by high speed machining and, on the other hand, laboratory specimens. The surfaces under tensile loading of the laboratory specimens have been machined using a shaper. Even if no more used in industrial machining, the shaper uses a process of cut similar to that of a lathe. Moreover, its straight cut process, yielding parallel straight grooves, allows taking into account the direction of machining grooves. Machining parameters have been chosen in order to generate various groove direction (UL specimens: perpendicular to the loading direction; UT specimens: parallel to the loading direction), various roughness (11 and 12 specimens: low roughness; 21 and 22 specimens : high roughness) using various cutting speed. Table 2 presents the various surface preparations of laboratory specimens. This set of specimens has been used to settle the modelling presented in section 4. Surface generation and preparation of industrial specimens have been conducted according to many different milling processes: face milling, shoulder milling, slot milling, finish plain milling, finish end milling, each with an up or down milling strategy. For each category, tool geometry and machining parameters (such as cutting speed or feed rate for instance) varied. Thirty different types of surfaces were so generated by high speed machining. These industrial specimens have been used for the validation step of the model.

Specimen reference	Ra T direction ( $\mu\text{m}$ )	Ra L direction ( $\mu\text{m}$ )	Cutting speed (m/mn)	Residual stress T direction (MPa)	Groove direction
UL11	0.5	n.a.	12	-137	
UL12	0.5	n.a.	50	-45	
UL21	7	n.a.	12	-54	
UL22	7	n.a.	50	-21	
UT11	0.25	0.5	12	-172	
UT21	0.35	7	12	-152	
UT22	0.3	7	50	-29	

**Table 2 : Summary of the surface preparation of the laboratory specimens**

## 2.2. Surface measurements

Residual stresses have been measured using X-ray diffraction technique with ASTX2001 device. The so-obtained values of residual stresses are given within +/- 30MPa. Concerning the geometrical characterization of the surfaces, a Mahr (Perthometer PKG-120) contour and roughness measuring system has been used. It is a diamond stylus instrument that can give conventional roughness parameters ( $R_a$ ,  $R_t$ ,  $R_q$ ...) and surface topography thanks to an automatically moving table. Horizontal resolution was  $0.5\mu\text{m}$  while height accuracy was  $0.1\mu\text{m}$ . 2D profiles used for the finite element analysis were 17.5mm long in the T direction for each specimen. This length has been chosen to get enough information whatever the studied surface.  $R_a$  data in L direction for UL specimens is not relevant for the present study because this roughness (in L direction) is not supposed to have an effect on the local loading. For UT specimen, they are just given as information to compare the surface conditions.



### **2.3. Fatigue testing**

Four-point bending tests have been conducted at room temperature in order to explore fatigue lives around  $10^5$  cycles. Tests were performed with a load ratio  $R=0.1$  and a frequency of 10Hz.

## **3. Preliminary results**

### **3.1. Surface measurements**

Conventional roughness parameter  $R_a$  and transversal residual stresses are presented in Table 2 for laboratory specimens. Concerning industrial specimens, the various machining conditions lead to surface roughness ranging from 0.1 to  $11\mu\text{m}$  in terms of  $R_a$ . It is important to note that, with the means of investigation that were used (microscopic observation and micro-hardness measurements) no change of the surface microstructure has been detected, whatever the machining process and machining parameters. For laboratory specimens, residual stresses are compression stresses, ranging from -20 to -175 MPa. As expected [15][16], residual stresses are linked to cutting speed: for a given set of machining parameters, compressive stresses are higher when the cutting speed is lower.

### **3.2. Fatigue tests**

SN curves of all laboratory specimens are presented in Figure 4. The influence of surface condition on the fatigue life is more important for high cycle fatigue ( $N_f > 3 \cdot 10^5$  cycles). Roughness has a predominant influence on the fatigue life. For UL specimens, for instance, low roughness specimens (UL12) have better fatigue strength than high roughness specimens (UL21) for approximately the same residual stresses. In addition, for a given roughness, residual stresses only seem to have a slight influence on the fatigue life: UL11 and UL12

exhibit the same fatigue behaviour. The same remark applies to the couples UT11 / UT21 and UT21 / UT22 respectively. However, the geometric roughness parameter  $R_a$  is not able to fully describe the difference in fatigue strength between all the samples. For such highly textured surfaces, it highly depends on the direction of the assessment length, as seen in Table 2 for UT specimens. It is then difficult to consider it as a reliable reference parameter. Even if a “correct” value of  $R_a$  is defined, for instance with respect to the loading direction, this parameter hardly can help to clearly quantify the relative position of the SN curves for all the specimens.

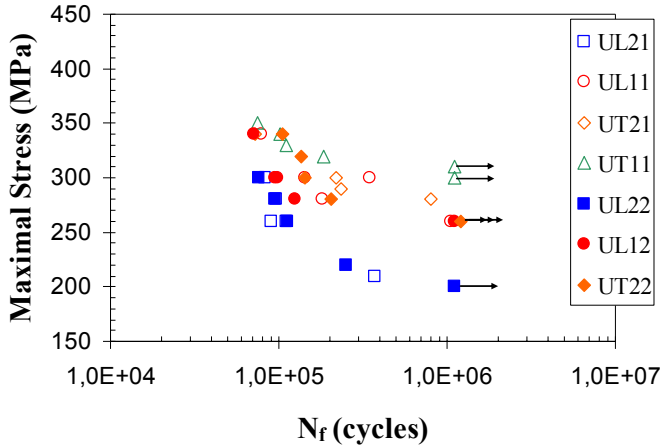


Figure 4 : SN curves for the various surface conditions

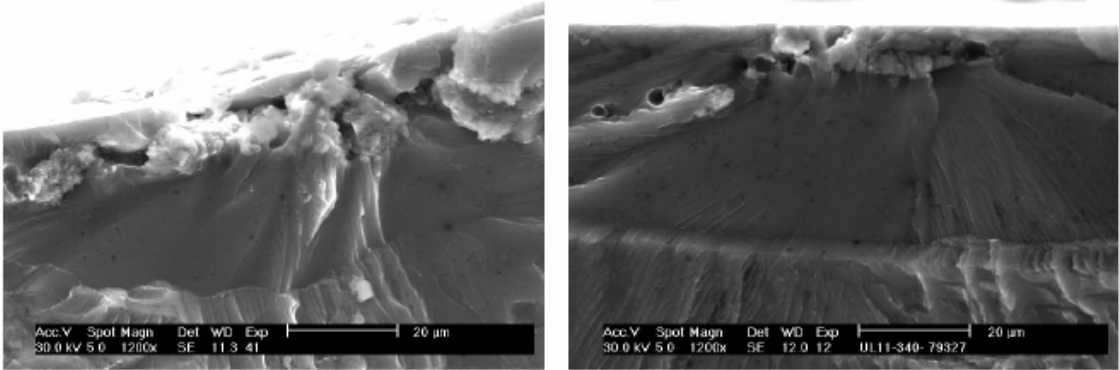


Figure 5 : Fracture surfaces of UT specimen (left) and UL specimen (right)

Fracture surfaces observations (Figure 5) show that whatever the specimen and the load level, fatigue cracks initiated on microstructural defects (essentially intermetallic inclusions and sometimes porosity) located on the flat loaded surface (within 20µm under the surface) and at the bottom of the machining grooves (when grooves are perpendicular to the loading). This is consistent with the observations that can be found in literature [17]. These defects were included in small recrystallized grains.

#### 4. Modelling the influence of surface roughness

##### 4.1. Effect of local stress concentration

As noted by many authors [8,9,13], standard purely geometric surface roughness parameters are not able to correctly describe the effect of roughness on the fatigue life of the investigated aluminium alloy. In the following, surface roughness is supposed to generate local stress concentration. However, this effect is not considered in terms of notch effect through the fatigue stress concentration factor  $K_f$  but is integrated in a fracture mechanics modelling. As noticed in section 3.2., the effect of surface roughness is different according to fatigue life time. Therefore, different modelling is proposed to predict fatigue. For fatigue limit the chosen model relies on the non propagation of an initial crack (or defect). According to linear elastic fracture mechanics the fatigue crack propagation threshold can be expressed with the following equation:

$$\Delta K_{th} = F \Delta \sigma_{th} \sqrt{\pi a} \quad (8)$$

where  $a$  is the crack length,  $F$  is a shape factor and  $\Delta \sigma_{th}$  is the minimum stress range required to propagate such a crack. Supposing the initial crack is located at the bottom of a machining groove and is very small, the stress concentration effect affecting the stress at the crack tip leads to

$$\Delta K_{th} = F K_t \Delta \sigma_{app} \sqrt{\pi a} \quad (9)$$

The fatigue limit can then be derived by considering it as the minimum stress range that can be applied without involving any propagation of an initial defect:

$$\Delta\sigma_D = \frac{\Delta K_{th}}{FK_t \sqrt{\pi a}} \quad (10)$$

With the following hypotheses, the fatigue limit is then quite easy to evaluate and only depends on the stress concentration factor:

1. the threshold stress intensity factor range  $\Delta K_{th}$  does not depend on the surface condition as whatever the machining parameters, metallurgical evolution has not been detected for the investigated alloy. Its value can be found in data base ( $\Delta K_{th}=3.5\text{MPa m}^{1/2}$ ) [18].
2. Initial crack or defect does not depend on the surface condition. Indeed, as noted in section 3.2., failure initiation always occurred on intermetallic inclusion within a re-crystallized grain, whatever the surface conditions. According to these observations, initial crack (defect) length  $a$  is considered to be the re-crystallized grain size in S direction, that is to say  $40\mu\text{m}$ . In the same way, the shape factor  $F$  is supposed to be identical whatever the surface condition and is roughly 1.12 for small cracks [19].

For limited fatigue lives, the roughness effect is different than for fatigue limit. This is attributed to crack propagation which constitutes the main part of fatigue life time. Machining process and subsequent roughness only have influence on the crack propagation in surface. Therefore, crack propagation in surface (along L direction) and in depth (along S direction) are treated separately. In the case of a semi elliptical crack the stress intensity factor can be expressed according to Newman and Raju [19]:

$$K_{I\phi} = f(a, c, \phi, W, t) \sigma \sqrt{\pi a} \quad (11)$$

where  $a$  and  $c$  are respectively the half short axis length and half long axis length of the crack,  $\phi$  is the angle (compared to the long axis) for which  $K$  is calculated,  $W$  is the specimen width

and  $t$  the specimen thickness. The detailed expression of  $f$  function can be found in [19]. It is supposed that a crack propagates in surface (increasing  $c$ ) and in depth (increasing  $a$ ) according to Paris law:

$$\frac{da}{dN} = C(\Delta K_{90^\circ})^m \quad \frac{dc}{dN} = C(\Delta K_{0^\circ})^m \quad (12)$$

with  $C$  and  $m$  material constants that can be found in database ( $m=3.41$ ,  $C=3.17 \cdot 10^{-11}$  (m/cycle)/(MPa $\sqrt{m}$ ) $^m$  in the present case). The main hypothesis is then that surface roughness generates stress concentration that only alters the surface crack propagation and the Paris law becomes:

$$\frac{da}{dN} = C(\Delta K_{90^\circ})^m \quad \frac{dc}{dN} = C(K_t \Delta K_{0^\circ})^m \quad (13)$$

An iterative calculation is then performed and, for each cycle,  $a$  and  $c$  are calculated and their new values are used to evaluate  $\Delta K_{90^\circ}$  and  $\Delta K_{0^\circ}$ . Initial crack size is re-crystallized grain size with an elliptical shape ratio  $a/c=0.5$  according to fracture surfaces observations. This grain size is considered as an long initial crack size (as required by Paris law) because fracture surfaces exhibit homogeneous features after the first grain fracture. Calculation is stopped when either  $a=t$ ,  $c=W$  or  $K_\phi=K_{IC}$  that is to say when crack either propagates through the thickness, through the width or is unstable. The number of iterations (cycles) is then considered as the crack propagation life ( $N_p$ ). Therefore, ( $N_p$ ) can be evaluated if the stress concentration factor associated with surface roughness is known. Afterwards an estimate of the crack initiation life ( $N_i$ ) can be obtained using a reference SN curve. This reference SN curve has been provided by the industrial partner (specimen shape and loading similar to those used in this paper) and has been chosen because the roughness-induced stress concentration factor of the specimens was equal to one. For each load level, crack propagation life time ( $N_p$ ) is then calculated according to the method previously presented with the appropriate stress concentration factor ( $K_t=1$ ). Considering total life time is the sum of crack

propagation life time and crack initiation life time,  $N_i$  is estimated for each load level by subtracting  $N_p$  from the experimental total life time given by the reference SN curve.

Assuming the crack initiation life time can be expressed according to a Basquin type power law [14]:

$$N_i = \beta(K_t \sigma)^\alpha \quad (14)$$

$\beta$  and  $\alpha$  are easily determined by plotting  $N_i$  as a function of the load level  $\sigma$ . These values of  $\beta$  and  $\alpha$  ( $\beta=8.08$  and  $\alpha=9.02E24$ ) are then used to determine  $N_i$  by Eq.(14) whatever the specimen and the load level.

As a conclusion for this part, it appears that whatever the SN curves area, fatigue life prediction via the chosen modelling requires determining the stress concentration factor  $K_t$  that characterizes the surface conditions.

## **4.2. Finite element analysis of surface topography**

In most of the recent approaches presented in the literature [7,8,13], the stress concentration factor  $K_t$  is calculated from averaged geometrical parameters of the surface. In the present study, the estimate of  $K_t$  based on measurements of the surface topography has been preferred.  $K_t$  is found by finite element analysis of the measured surface topography and is then supposed to lead to a stress condition which is more representative of what really undergo the samples. This way of characterizing a surface topography from a mechanical point of view without the use of geometrical parameters gave place to a patent [20]. A similar approach has also been proposed by As et al. [9]. 2D profiles that are measured are recorded with a sampling rate of  $1\mu\text{m}/\text{point}$ . From the 17000 points that are recorded, only 800 points are regularly extracted and interpolated with a spline function to be used in the finite element modelling. As seen in Figure 6, this results in a filtered profile where second order roughness (induced by tool edge defects for instance) is not taken into account. This filter has been

chosen because stress concentration generated by second order roughness is supposed to be not significant, from a fatigue point of view, compared to stress concentration generated by first order roughness (due to tool shape and machining parameters).

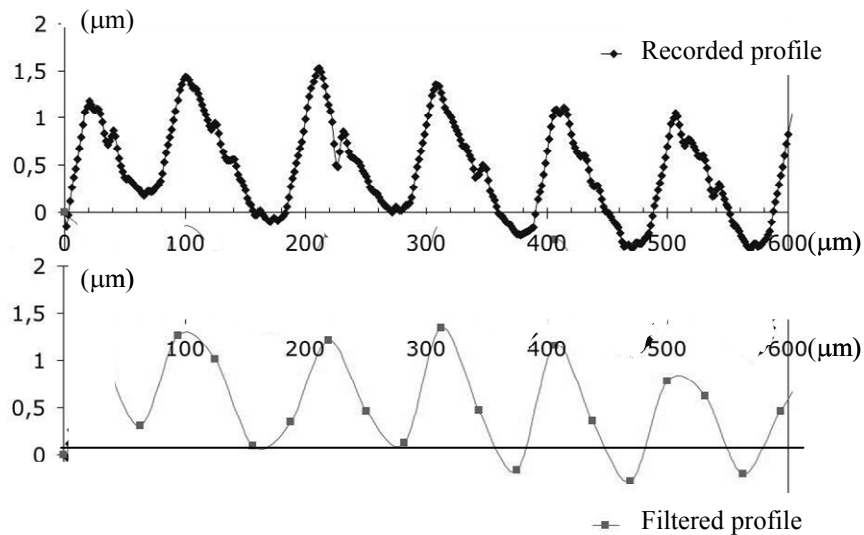


**Figure 6 : Example of recorded and filtered profile of surface specimen**

This profile is then used as surface model to generate the finite element geometry. Material behaviour is linear elastic. Plane strain hypothesis is supposed for this 2D calculation. Triangular elements with quadratic interpolation are used for the mesh. Elements size is roughly 30 μm. For this filtered profile, it has been shown this mesh size leads to convergence of the numerical results [21]. Problems of validity of continuum mechanics and of the hypothesis of isotropic and homogeneous material induced by extremely refined mesh, such as pointed out by As et al. [9], are so avoided. Uniform load is applied as boundary conditions. The maximal Von Mises equivalent stress obtained by the calculation is then divided by the nominal Von Mises equivalent stress due to the applied load to classically determine the stress concentration factor  $K_t$ . Due to regularity of grooves, this  $K_t$  value is generally found in most of the valleys of the measured surface topography. An example of finite element calculation performed to determine  $K_t$  is shown in Figure 7. In this figure, it can be seen the depth of the surface layer affected by the stress concentration is of the same order

of magnitude as the recrystallized grain size considered as the initial crack size used in the previous model calculating ( $N_p$ ). This supports the hypothesis that crack propagation in depth is not affected by the stress concentration (Eq.13). On the contrary, considering propagation in surface (along L direction),  $K_t$  calculated by the 2D finite element analysis is supposed to affect all the sample width in a similar way, supporting hypothesis of Eq. 13. For laboratory specimens (where grooves are parallel), it is obviously close to reality. For milled specimen tested in section 4.4., the previous conditions are locally relevant for initiation step and beginning of crack propagation (high groove radius compared to grain size). When crack propagates from a macroscopic point of view, the crack follows the envelope of the grooves that can be assimilated to a straight line.

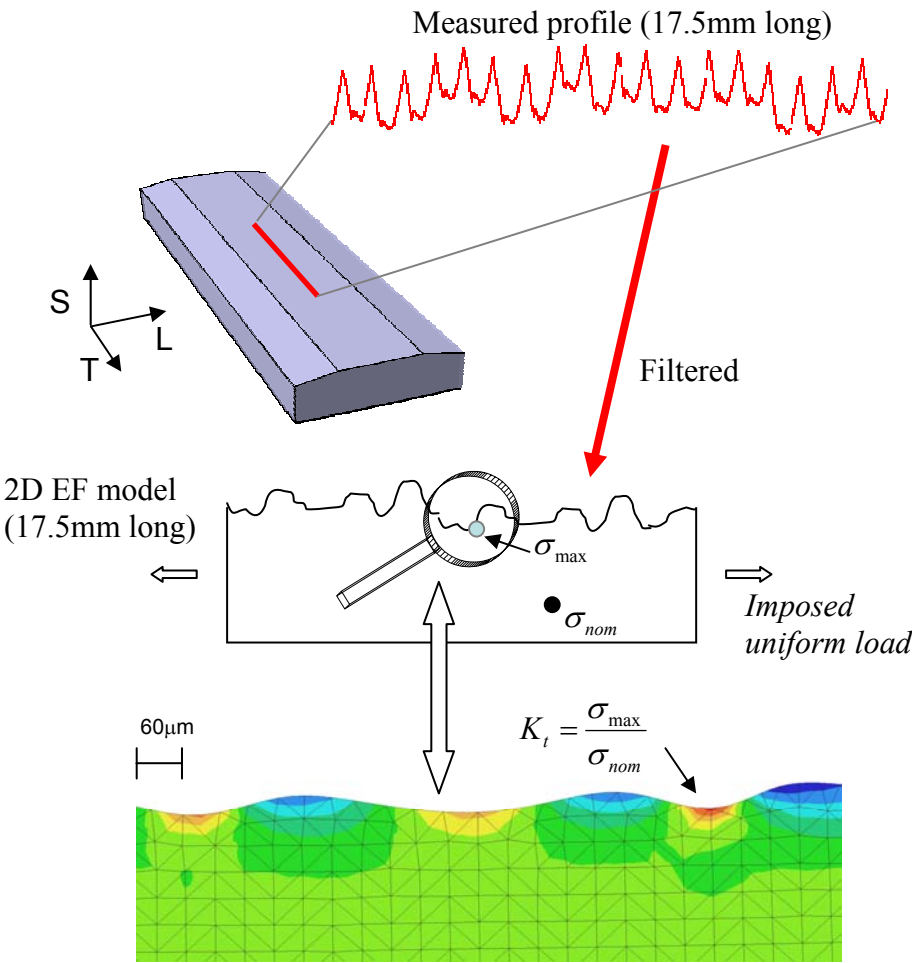


**Figure 7 : Principle of finite element calculation to determine stress concentration factor**



### 4.3. Results

For each specimen, the stress concentration factor  $K_t$  characterising the surface conditions is calculated according to the previous process presented in section 4.2. The so-obtained values are then used in Eq. (10) to determine the fatigue limit of each type of specimen. The results are presented in Figure 8. Calculated fatigue limits are in good agreement with the experimental ones for all the specimens. For limited fatigue lives, the total number of cycles to failure is calculated with

$$N_f = N_i + N_p \quad (15)$$

where  $N_i$  is determined via Eq. (14) and  $N_p$  is estimated by the iterative calculation using Eq. (13). The so-obtained results are compared with experimental data in the SN curves presented in Figure 9 and Figure 10. Fatigue limits (from Figure 8) are also included to get a global assessment of the complete modelling: predicted curves have been linked at their intersection, close to  $3 \cdot 10^5$  cycles. Experimental results and predicted fatigue life time are in very good agreement for all types of specimens. In addition, it is noteworthy that shape and size of fatigue portion of the fracture surface determined by post-mortem observations fit to the numerical calculations giving  $N_p$ . The maximal error, observed for UT11 specimens in Figure 10, comes from the reported fatigue limit (10% error in Figure 8). In that case, the limits of the modelling may have been reached. Indeed, for such specimens with groove direction parallel to the loading direction,  $K_t$  is very low. In addition, for UT11, compressive residual stresses are particularly high (see Table 2). The hypothesis considering the effect of surface texture is predominant compared to the other surface parameters may not be valid in that case and may lead to under-estimate the fatigue limit.

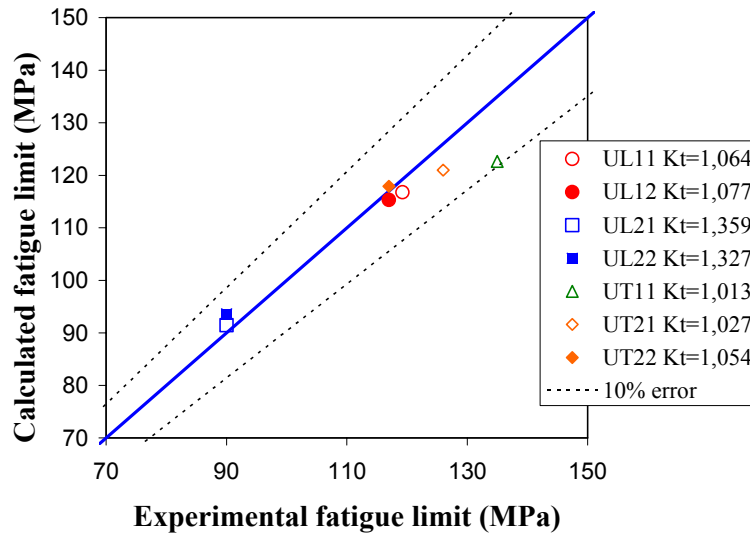


Figure 8 : Calculated fatigue limit compared to experimental fatigue limit ( $N_f = 10^6$  cycles)

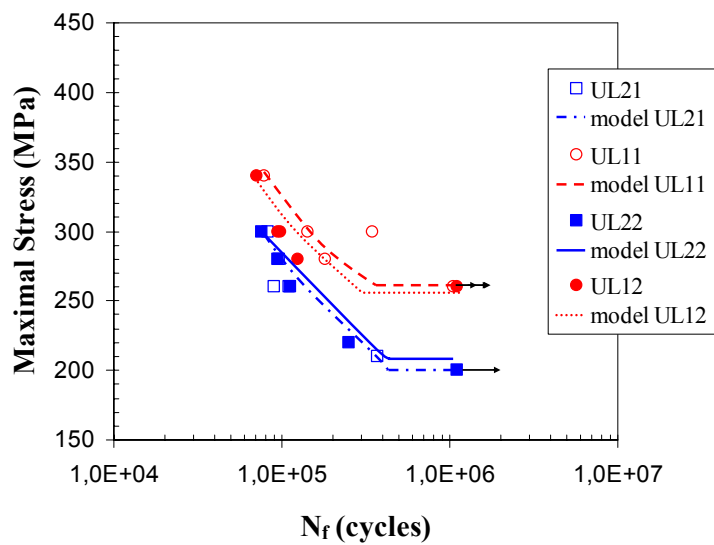
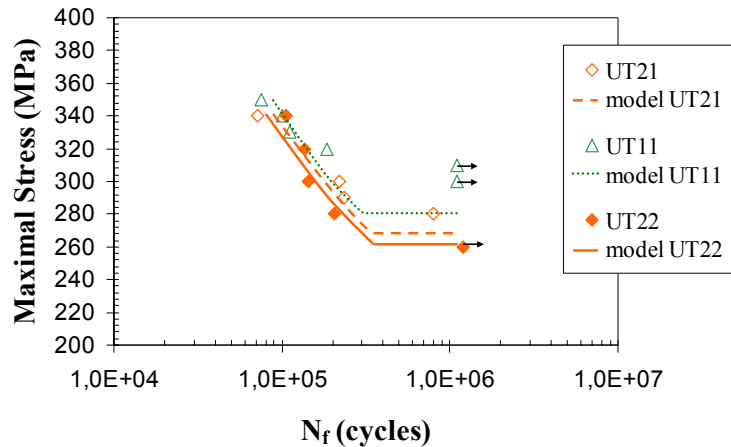


Figure 9 : Predicted fatigue life time compared to experimental SN curves for UL specimens



**Figure 10 : Predicted fatigue life time compared to experimental SN curves for UT specimens**

#### 4.4. Validation

As seen in the previous section, the proposed model based on  $K_t$  obtained by the finite element analysis of the measured topography of surface specimens fits well with the experimental fatigue curves of samples machined by a shaper. However this machining process, which leads to parallel grooves, is no more used in industrial production where the surface generation is more complicated. In order to assess the relevance of the present approach in industrial cases, the whole method (from the measure of the surface to the fatigue life prediction, via the determination of  $K_t$ ) has been applied to specimens and fatigue data provided by an industrial partner. Experimental SN curves and predicted SN curves are compared in Figure 11 for two categories of high speed machined specimens: fine shank-end milled specimens ( $R_a=0.25\mu\text{m}$ ) and rough ball-end milled specimens ( $R_a=11.1\mu\text{m}$ ). As an indication the  $K_t$  values from the finite element analysis are given in Figure 11 for each category. It is noteworthy that for these two extreme types of surface in terms of  $R_a$ , the predictions give good results.

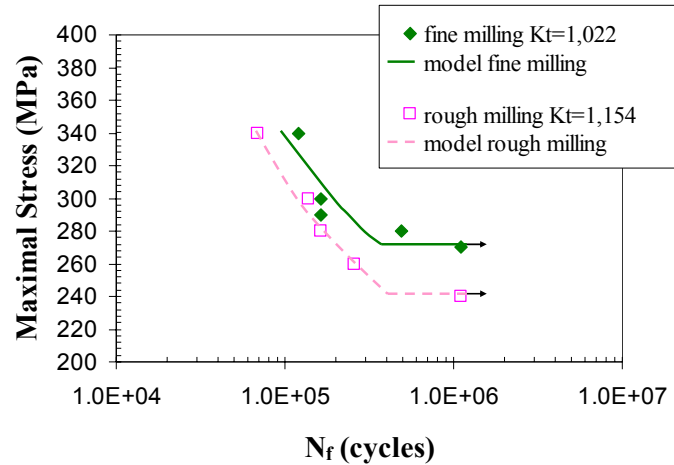


**Figure 11 : Predicted fatigue life time compared to experimental SN curves for two kinds of high speed machined specimens**

All the other specimens have been tested in fatigue by the industrial partner with a load ratio 0.1 and with a maximal stress of 320 or 300MPa. After testing, the surface topography of one specimen of each category of machining was measured in the laboratory and the  $K_t$  was next calculated. It was then supposed to be the same for all the specimens of the considered category. Figure 12 and Figure 13 present the experimental and predicted fatigue life time as a function of  $K_t$  respectively for tests with a maximal stress of 320 and 300MPa. Obviously, the model gives good results for the various samples. The scatter observed for low  $K_t$  values can result either from the scatter of fatigue data or from the fact that  $K_t$  has not been evaluated for each specimen but only for one specimen of each category. Therefore, changes of the surface topography due to possible wear of tools is not taken into account. From all these results it appears that the proposed approach, even if settled from laboratory specimens, is relevant in industrial cases for the investigated alloy.

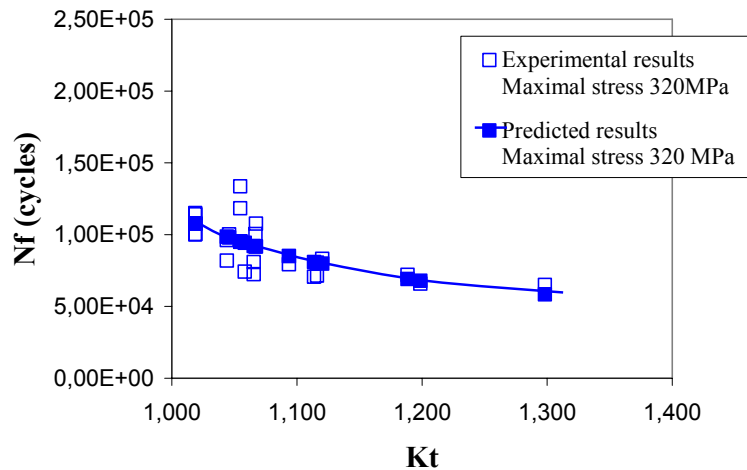


**Figure 12 : Predicted and experimental fatigue life time versus  $K_t$  for high speed machined specimens with various machining conditions – Maximal stress 320MPa**

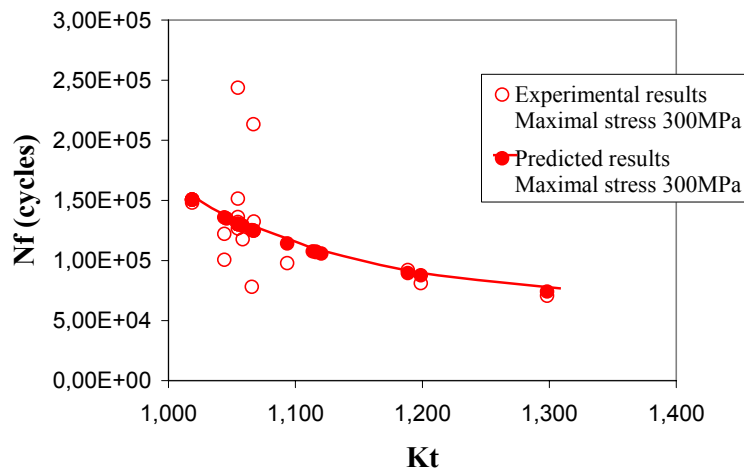


**Figure 13 : Predicted and experimental fatigue life time versus  $K_t$  for high speed machined specimens with various machining conditions – Maximal stress 300MPa**

## 5. Conclusion

For the present Al alloy and for the machining processes that have been investigated, the influence of machined surface condition on the fatigue behaviour is due to a predominant effect of roughness. In order to model this effect, surface topography is characterized from a mechanical point of view without the use of geometrical parameters: stress concentration factor  $K_t$  is calculated by finite element analysis from surface measurements. This so-called stress concentration factor is integrated in two different modelling to predict

limited fatigue lives and fatigue limit. In addition to this calculated  $K_t$ , these two modelling only require basic fatigue crack propagation data (fatigue threshold and Paris law parameters). The whole approach (measurement of surface topography, determination of  $K_t$ , fatigue life prediction) provides a reliable mean to predict fatigue life of components machined in the present alloy when changing machining parameters and processes in an industrial frame without time-consuming and expensive tests. Further investigation is necessary to define the validity area of this global modelling. In particular, it could be interesting to test this method with a larger range of machining processes. Changing the material could also lead to adapt this approach in terms of  $K_t$  calculation or fatigue model and to extend it to combined effects of roughness, microstructure and residual stress.

### **Acknowledgements**

The authors gratefully thank Airbus France and particularly Vivien Vergnes for supplying material and specimens with various machining conditions.

### **References**

- [1] Shigley J, Mischke C, Budynas R. Mechanical Engineering Design. 7<sup>th</sup> edition. McGraw-Hill, 2003
- [2] Henaff G, Morel F. Fatigue des structures : endurance, critères de dimensionnement, propagation des fissures, rupture. Ellipses, 2005
- [3] Maya PS. Geometrical characterization of surface roughness and its application to fatigue crack initiation. Material Science and Engineering 1975;21:57-62
- [4] Maya PS. Effects of surface roughness and strain range on the low-cycle fatigue behavior of type 304 stainless steel. Scripta Metallurgica 1975;9:1277-1282
- [5] Wiesner C, Kunzi HU, Ilshner B. Characterization of the topography of turned surfaces and its influence on the fatigue life of AL-7075. Material Science and Engineering A 1991;145:151-158
- [6] Peterson RE. Stress concentration factors. New York : John Wiley and Sons, 1974
- [7] Arola D, Ramulu M. An examination of the effects from surface texture on the strength of fiber-reinforced plastics. J. Compos Mater 1999;33(2):101-86
- [8] Arola D, Williams CL. Estimating the fatigue stress concentration factor of machined surfaces. Int Jnl Fatigue 2002;24:923-930.

- [9] As SK, Skallerud B, Tveiten BW, Holme B. Fatigue life prediction of machined components using finite element analysis of surface topography. *Int Jnl Fatigue* 2005;27:1590-1596.
- [10] Murakami Y. *Metal fatigue : effects of small defects and non-metallic inclusions*. Elsevier Science;2002.
- [11] El Haddad MH, Dowling NF, Topper TH, Smith KN. J integral applications for short fatigue cracks at notches. *Int J Frac* 1980;16(1):15-24.
- [12] Taylor D, Clancy OM. The fatigue performance of machined surfaces. *Fat Fract Eng Mater* 1991;14(2/3):329-336.
- [13] Andrews S, Sehitoglu H. A computer model for fatigue crack growth from rough surfaces. *Int Jnl Fatigue* 2000;22:619-630.
- [14] Bathias C, Bâillon JP. *La fatigue des matériaux et des structures*. 2<sup>nd</sup> edition. HERMES. Paris, 1997
- [15] Tsuchida K, Kawada Y, Kodama S. A study on the residual stress distributions by turning. *Bulletin of the JSME* 1975;18(116):123-130.
- [16] Jang DY, Seireg AA. A model for predicting residual stresses in metal cutting. *Proceedings of Japan Int Tribology Conf. Nagoya*.1990:439-444.
- [17] Patton G, Rinaldi C, Bréchet Y, Lormand G, Fougères R. Study of fatigue damage in 7010 aluminium alloy. *Mat Sci Eng A* 1998;254:207-218.
- [18] Zitounis V, Irving PE. Fatigue crack acceleration effects during tensile underloads in 7010 and 8090 aluminium alloys. *Int Jnl Fatigue* 2007;29(1):108-118.
- [19] Newman JC, Raju IS. Stress intensity factor equations for cracks in three dimensional finite bodies subjected to tension and bending loads. *NASA Technical Memorandum*, 1984.
- [20] Chieragatti R, Suraratchai M, Mabru C, Espinosa C, Vergnes V. Procédés de caractérisation de la tenue en fatigue d'une pièce à partir de son profil de surface. *French Patent n°0650793*, 2006.
- [21] Suraratchai M, Influence de l'état de surface sur la tenue en fatigue de l'alliage d'aluminium 7010. *PhD thesis, Université Toulouse III, France*, 2006.